Metallic Ni nanoparticles embedded in hierarchical mesoporous Ni(OH)$_2$: A robust and magnetic recyclable catalyst for hydrogenation of 4-nitrophenol under mild conditions

Ningxin Zhang [a], Xiangwen Wang [b], Longlong Geng [a,*], Zhongmin Liu [a], Xiuling Zhang [a], Chunhui Li [a], Dashuai Zhang [a], Zhigang Wang [a], Guoming Zhao [c]

[a] College of Chemistry and Chemical Engineering, Dezhou University, Dezhou 253023, China
[b] Dezhou Vocational and Technical College, Dezhou 253034, China
[c] College of Chemical and Environmental Engineering, Shandong University of Science and Technology, Qingdao 266590, China

ARTICLE INFO

ABSTRACT

The design of non-noble metal catalysts with high catalytic activity and stability is highly important for heterogeneous catalysis. Herein, we report a kind of Ni nanoparticles embedded in a 3D nanoarchitecture of Ni(OH)$_2$, which was synthesized via an solid state redox strategy. The obtained material exhibited an interconnected pore structure and high surface area, thus displaying excellent catalytic activity and stability for the hydrogenation of 4-nitrophenol (4-NP) under mild conditions (1 atm and room temperature). The reaction rate constant and activation energy of the catalyst were determined to be 151.3×10^{-3} min^{-1} and 42.3 kJ mol^{-1}, respectively. Moreover, Ni/Ni(OH)$_2$ also exhibited relatively high superparamagnetism properties; it could be separated facilely by using an external magnet and could be reused for at least ten times without obvious deactivation, exhibiting high reusability.

© 2019 Elsevier Ltd. All rights reserved.

1. Introduction

Nitroarenes are a class of important nitrogen compounds and ubiquitous intermediates, which are widely used in biological, agricultural, and pharmaceutical synthetic processes [1–4]. The catalytic hydrogenation of nitroaromatic compounds over a Pt- or Au-based catalyst is the traditional method for arylamine synthesis [5–8]. In view of the high synthetic cost, as well as the increasing demand of arylamine in practical organic synthesis, developing new and low-cost materials to replace the traditionally-used noble metal catalysts is highly important.

Nickel (Ni), as an important element in the family of transition metals, shows great promising potentials in heterogeneous catalysis owing to its distinct electronic properties [9–11]. Nickel has the advantages of low-cost and ready availability, and Ni-based materials with various size, shape, structure, and composition have been demonstrated to be active in some hydrogenations of organic compounds, such as olefins, aldehydes, ketones, and so on [12–15]. What's more, these catalysts could be recycled using a magnet due to its intrinsic paramagnetism property [16,17], particularly for

liquid phase reactions. The shortcoming for practical application is their relatively low stability. For example, despite efficient catalytic performance being obtained over some supported Ni-NPs, most of these catalysts need to be stored without oxygen because of the low antioxidant ability of the Ni species in the air [18,19]. Additionally, activation under reductive atmosphere is usually necessary before some hydrogenation reactions [19,20]. As a result, the active Ni species, especially for small Ni particles, trend to aggregate irreversibly during preparation and catalytic reactions because of their high surface energies, leading to dramatic losses in catalytic activity [21–25]. Therefore, it is keenly desired to develop a high-efficiency and stable Ni catalyst for hydrogenation processes.

With above considerations in mind, if another material can be introduced on the surface of Ni NPs to form an embedded structure, the aggregation of small particles can be inhibited and the oxidation process may be slowed down. In this work, we reported the synthesis of Ni-NPs embedded in a hierarchical Ni(OH)$_2$ nanoarchitecture (Ni/Ni(OH)$_2$) via a one-pot solid state redox method. The obtained Ni/Ni(OH)$_2$ catalyst possessed a hierarchical mesoporous structure and large special surface area, which exhibited excellent performance in hydrogenation of 4-NP even under at room temperature. Meanwhile, the embedded structure leads to a great enhancement in the stability of the obtained catalyst, which

could be reused for more than ten times without obvious fading in activity. In addition, the catalyst also possesses relatively high superparamagnetism; it could be facilely recovered from the liquid reaction mixture using an external magnet, exhibiting relatively high reusability.

2. Experimental

2.1. Materials and preparation of catalysts

All chemicals were of analytical grade and used without further purification. The catalyst was synthesized using a solid state redox method under ambient conditions. In a typical synthesis, NiCl$_2$·6H$_2$O (5.0 mmol), NaBH$_4$ (2.0 mmol), NaOH (8.0 mmol) and NaCl (4.0 g) were mixed in an agate mortar at room temperature. After grinding for 10 min, ten drops (1 mL) of water were added slowly and grinding resumed for another 20 min. The color of the mixtures changed from light green to black accompanied by the release of heat and vapor. The mixtures were dried at 60 °C and washed with distilled water thoroughly to obtain the final catalyst.

For comparison, Ni(OH)$_2$ and Ni/Ni(OH)$_2$ were synthesized using the same method without the addition of NaBH$_4$ and NaCl. In addition, Ni-NPs were also synthesized using the same method without the addition of both NaOH and NaCl.

2.2. Catalyst characterizations

The morphology and microstructure of the synthesized materials were examined using scanning electron microscopy (SEM, S-4800, Hitachi) and transmission electron microscope (TEM, FEI Tecnai F20 EM). X-ray diffractometer (XRD) with Cu Kα source (λ = 1.5418 Å) was carried out to detect the crystalline structures of the catalysts. X-ray photoelectron spectroscopy (XPS) was used to study the electronic property of the catalysts on a Thermo ESCA LAB 250 system (Mg Kα, 1254.6 eV). The N$_2$ adsorption isotherms were performed at 77 k using a Micromaterial ASAP 2010N analyzer. Before measurements, the samples were degassed at 150 °C for 20 h. Brunauer–Emmett–Teller (BET) model was used to calculate the specific surface area. Using the Barrett–Joyner–Halenda (BJH) model, the pore size distribution was evaluated from the desorption branch of the nitrogen isotherm. Magnetic measurements were tested using SQUIDVSM magnetometer at room temperature.

2.3. Catalytic hydrogenation of 4-nitrophenol

The catalytic properties of the obtained catalyst were investigated by using 4-NP hydrogenation as a model reaction. The reaction was performed at room temperature (25 °C) and atmospheric pressure using NaBH$_4$ was reducing agent. In general, 10 mL of fresh NaBH$_4$ solution (0.1 M) and 20 mL of 4-NP solution (0.1 mM) was first mixed to obtain the yellow-green solution. After the addition of 20 mg catalyst, the products were taken using a sampling pipe, and monitored by UV–Vis spectroscopy in a scanning range of 200–600 nm. The conversion of 4-NP was calculated based on the change of absorbance at 400 nm using $(A_0 - A_t)/A_0$, where A_0 and A_t represent the absorbance of reaction mixture at initial stage and intervals, respectively. Since a higher concentration of NaHB$_4$ than that of 4-NP was used during reaction, the rate of the catalytic reaction was evaluated using pseudo-first order kinetics. The rate constant (k) is calculated using the equation $\ln(A_t/A_0) = -kt$. In addition, based on the Arrhenius plot, the activation energy (Ea) of the reaction over the different catalysts was also calculated.

In the filtration experiment, the solid catalysts were separated with a Buchner funnel after reaction for 15 min, and the filtrate mixture was then put into the reactor for continuous reaction under the same conditions without the use of any solid catalyst. In the recycle test, the solid catalyst was separated from the reactants by an external magnet after reaction and repeat in the next reaction after washed with water.

3. Results and discussion

3.1. The fabrication and morphology of the obtained catalysts

The fabrication of the Ni/Ni(OH)$_2$ catalyst consists of thoroughly grinding of raw materials (nickel chloride, sodium borohydride and sodium hydroxide) in an agate mortar combined with a water washing treatment. Two reactions occurred during the catalysts synthesis: the nickel salts could react with sodium hydroxide to form nickel hydroxide (Eq. (1)); meanwhile, it could also be reduced by sodium borohydride to produce metallic nickel (Eq. (2)):

$$Ni^{2+} + 2OH^- \rightarrow Ni(OH)_2 \tag{1}$$

$$Ni^{2+} + 2BH_4^- + 6H_2O \rightarrow Ni\ +\ 2B(OH)_3 + 7H_2 \tag{2}$$
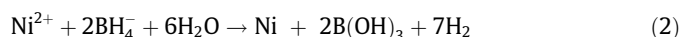
In addition, NaCl was added as an inert hard template during preparation, and it could dissolve easily in water during washing treatment, forming pores in the obtained materials [26,27]. The load amount of Ni is 20wt% based on the mole ratio of raw materials. Since the procedure is easy to perform and the starting material is nontoxic and inexpensive, the catalyst has the potential of mass production.

As shown in Fig. 1a, the scanning electronic microscopy (SEM) image reveals that Ni/Ni(OH)$_2$ exhibited a well-defined hierarchical architecture, which is similar to the reported samples fabricated using hard template routes [26–29]. The architecture is constructed of large member of sheet-like substrates, and the thickness is about 5–8 nm. In good agreement with the SEM results, low magnification TEM image (Fig. 1b) confirms the typical hierarchical architecture and wrinkled thin sheets. Large numbers of pores and distortions were interspersed among the architecture, which is beneficial for the diffusion of reactants during reaction process. Fig. 1c clearly reveals the Ni species present as 5–10 nm nanoparticles embedded in the Ni(OH)$_2$ substrate with relatively high dispersion. This unique structure could prevent their aggregation during the preparation and reaction processes. More detailed crystal structure was further investigated by high resolution transmission electron microscopy (HRTEM). As shown in Fig. 1d, the lattice fringes marked by the yellow lines and the measured lattice d-spacing are 0.20 and 0.28 nm, respectively, which are consistent with the interplane distance values of (1 1 1) plane of Ni and (1 1 0) plane of Ni(OH)$_2$ [28,29].

The Ni 2p XPS spectrum of Ni/Ni(OH)$_2$ was shown in Fig. 1e. The two main peaks at 852.3 and 855.8 eV could be assigned to Ni 2p 1/2 and Ni 2p 3/2 core level, indicating the valence state of Ni on the catalyst surface is mainly +2 [29,30]. In addition, only a weak peak assigned to the metallic nickel species was observed at the lower bonding energy (852.3 eV) [30,31]. In combination with the TEM results, this should be caused by the embedded nature of Ni NPs. This unique structure could prevent the partial oxidation of Ni-NPs during the preparation and reaction processes. The O 1s spectra can be deconvoluted into two peaks (Fig. 1f) based on the previous reports [32,33]. The peak centered at about 530.5 eV is related to the oxygen in the oxide lattices and, the second peak in the range of 530–535 eV can be assigned to the —OH species or oxygen vacancies in the catalyst [34,35]. It is clear that the area
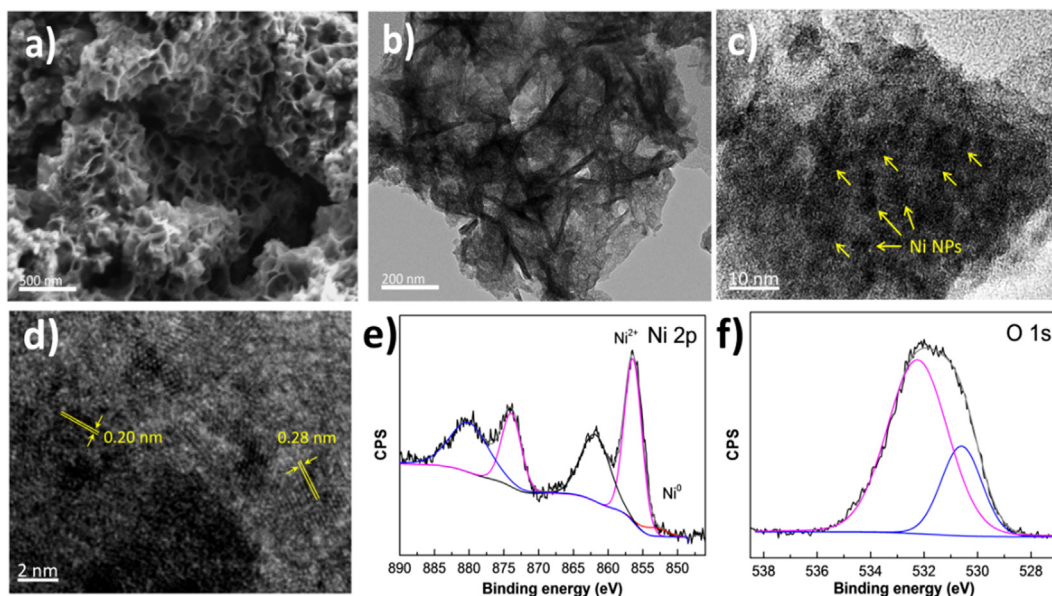
Fig. 1. SEM (a), TEM (b), HRTEM images (c and d) and XPS spectra (e and f) of the as-synthesized Ni/Ni(OH)$_2$ catalyst.

of the second peak is much larger than the first one, indicating the low degree of crystalline phases of the obtained material.

In addition, the magnetism of Ni species in Ni/Ni(OH)$_2$ was expected to allow easy separation of the catalysts from aqueous reaction media. As shown in Fig. 2, Ni/Ni(OH)$_2$ exhibited a super-paramagnetic character loop at room temperature. The saturation magnetization is 3.45 emu g^{-1} and the remnant magnetization is only 0.22 emu g^{-1}. These values are interesting, because catalyst could be easily separated by an external magnet and no magnetization remained after removing the magnetic field. The inset in Fig. 2 further confirms that Ni/Ni(OH)$_2$ could be easily separated from the aqueous mixture by an external magnet.

For comparison, Ni(OH)$_2$ and Ni NPs were also prepared in this work using the same procedure without the addition of sodium borohydride and sodium hydroxide. The phase structure of the obtained catalysts was confirmed by the SEM and XRD analyses. Ni(OH)$_2$ displayed a hierarchical architecture similar to that of Ni/Ni(OH)$_2$, meanwhile, irregular particles with a size of 30–50 nm were observed in the SEM image of Ni NPs (Fig. S1).
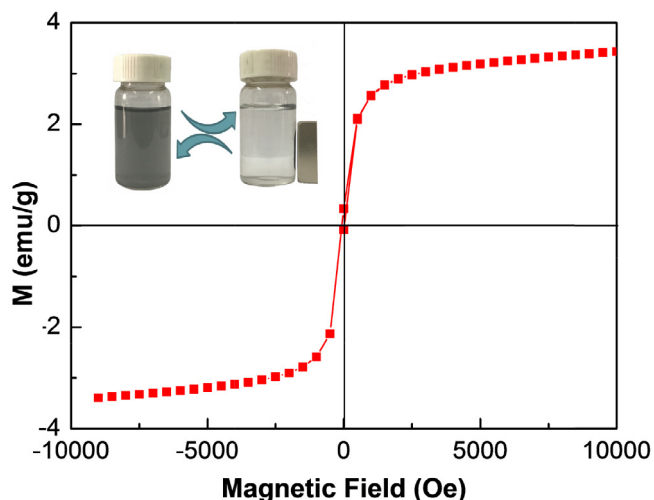
As displayed in Fig. 3a, two diffraction peaks at 33.6° and 59.6° can be found in the XRD patterns of Ni(OH)$_2$, which could be assigned to the diffractions from the (1 1 0) and (3 0 0) crystal planes of nickel hydroxide (JCPDS: 22-0444) [36,37]. However, two new peaks (2θ = 44.5° and 51.8°) assigned to (1 1 1) and (2 0 0) crystal planes of cubic Ni (JCPDS 04-0850) were observed in the XRD patterns of Ni NPs. As for Ni/Ni(OH)$_2$, the corresponding XRD pattern shows that the peaks belonging to both Ni(OH)$_2$ and Ni are observed, further confirming that the sample is a mixture of metallic Ni and nickel hydroxide. Additionally, the peaks are broad and low in intensity for all the samples, indicating the as-prepared catalysts are weakly crystalline.

N$_2$ adsorption–desorption isotherm and corresponding pore size distribution of the obtained Ni-based catalysts are shown in Fig. 3b–d. It shows that both Ni/Ni(OH)$_2$ and Ni(OH)$_2$ displayed a type IV isotherm with an H4 hysteresis loop in the relative pressure range 0.4–1.0, reflecting the presence of mesoporous structure [38,39]. As for Ni NPs, an H3 hysteresis loop in the pressure range 0.8–1.0 was observed, which could be assigned to the packing of Ni particles. It is notable that two mean pore diameters of 4.5 nm and 49.5 nm were observed in the BJH pore size distribution curve of Ni/Ni(OH)$_2$ (Fig. 3b, inset), further confirming the hierarchical mesoporous structure of this catalyst, which is in agreement with the SEM and TEM results. In addition, the surface area and pore volume of Ni/Ni(OH)$_2$ was 231.5 m^2·g^{-1} and 0.33 cm^3·g^{-1}, which was obviously bigger than that of the other samples (Table 1). It is noteworthy that the addition of NaCl plays an essential role in the fabrication of catalysts with hierarchical structure and high surface area. Without the addition of NaCl during material synthesis, the obtained material (designated as Ni/Ni(OH)$_2$−1) displayed not only a disordered structure, but also a relatively low surface area (see Figs. S1c, S2 and Table 1). Generally, a larger surface area is beneficial for the catalyst to expose more active sites, further improving the efficiency of the catalysts [40,41].

3.2. The catalytic activity and stability of the synthesized Ni-based catalysts

The results above confirm the successful synthesis of Ni/Ni (OH)$_2$ catalysts containing high surface area, interconnected mesoporous and a defect-rich structure. To evaluate their catalytic

Fig. 2. The magnetic hysteresis loop of Ni/Ni(OH)$_2$ under room temperature.
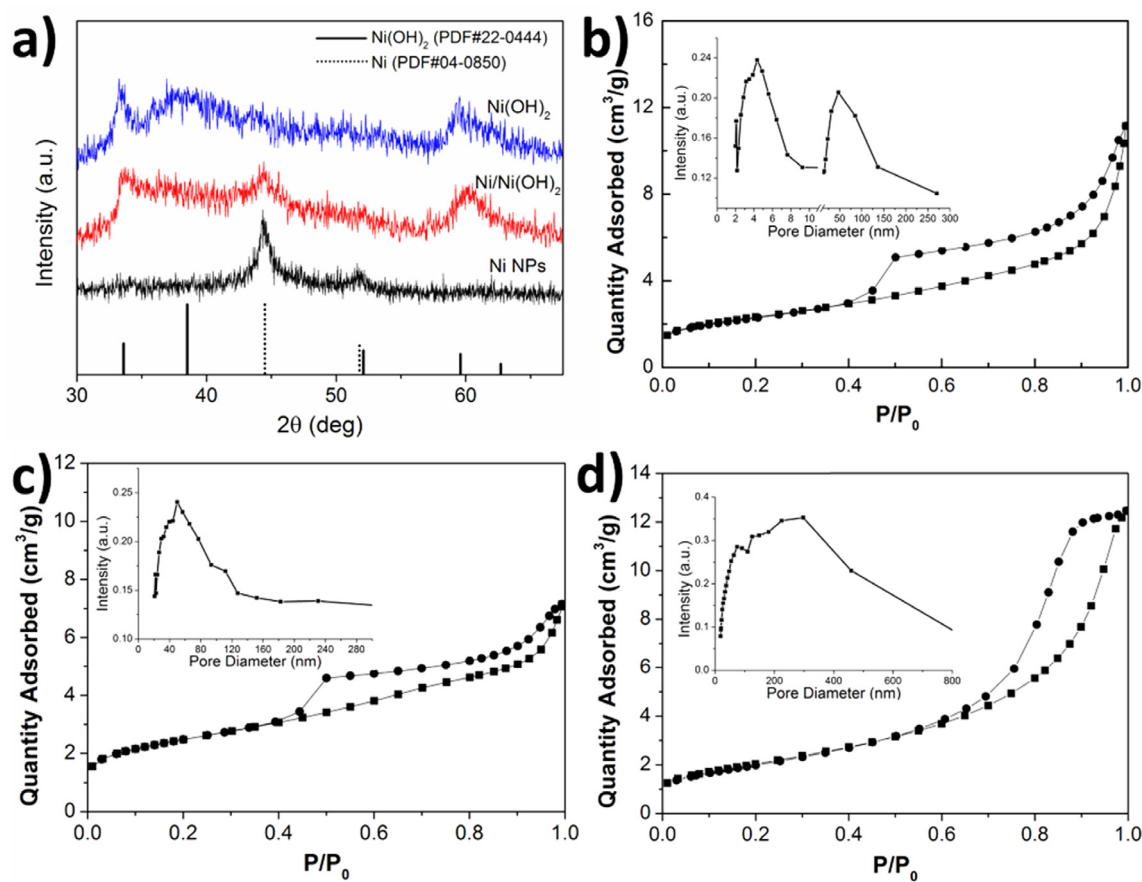
Fig. 3. XRD patterns (a) and N$_2$ adsorption–desorption isotherms and pore size distributions of the obtained catalysts: Ni/Ni(OH)$_2$ (b), Ni(OH)$_2$ (c) and Ni NPs (d).

Table 1
Texture properties of the synthesized Ni-based catalysts.

Sample	S_{BET} (m^2/g)	Pore volume (cm^3/g)	Pore diameter[a] (nm)
Ni/Ni(OH)$_2$	231.5	0.33	62.3
Ni(OH)$_2$	193.3	0.21	53.2
Ni NPs	129.2	0.11	98.2
Ni/Ni(OH)$_2$−1	104.1	0.19	39.8

[a] Average pore diameters calculated from adsorption branches using BJH model.

properties, the hydrogenation of 4-NP to 4-aminophenol (4-AP) was carried out using NaBH$_4$ as the reducing agent. Fig. 4a shows UV–Vis absorbance spectra for the hydrogenation of 4-NP in the presence of Ni/Ni(OH)$_2$. It is clear that the absorption peak at 400 nm gradually decreases in intensity along with the increase of a new absorption peak at 300 nm, indicating the reduction of 4-NP and formation of 4-AP, respectively [42,43]. A 98.9% conversion of 4-NP was obtained in only 40 min reaction over Ni/Ni(OH)$_2$ at ambient conditions (25 °C and 1 atm). Under the same conditions, a slight decrease was detected in the intensity of the absorption peak at 400 nm over Ni(OH)$_2$ (Fig. S3), indicating Ni(OH)$_2$ is not the main active phase for the title reaction. In addition, Ni/Ni(OH)$_2$−1 also displayed inferior activity compared to Ni/Ni(OH)$_2$ under same conditions (Fig. S3). Even with the support of solid Ni particles, the 4-NP conversion is only 54.2% in 40 min reaction. That is to say, Ni/Ni(OH)$_2$ undergo more efficient catalysis than solid Ni NPs. The inferior catalytic performance of Ni-NPs should be connected with their low anti-oxidative ability. As demonstrated by Jia et al., a thin NiO film may be generated due to the partial oxidation of surface Ni in an atmospheric environment

[44], which hinders the exposure and interaction of the active species with the reactants.

The reaction kinetics for the hydrogenation of 4-NP over the synthesized catalysts were also revalued (Fig. 4b). Since the amount of NaBH$_4$ is excessive compared to 4-NP in the catalytic reaction system, the reaction rate is roughly independent of the NaBH$_4$ concentration, and the kinetics can be considered pseudo-first-order with respect to the 4-NP only [42,45]. Based on the ln (A_t/A_0) values as a function of reaction time, the calculated rate constant (k) is 151.3 × 10^{-3} min^{-1} for Ni/Ni(OH)$_2$, which is about 25 and 12 times higher than those of Ni(OH)$_2$ and Ni NPs (the k value is 6.0 × 10^{-3} min^{-1} and 11.9 × 10^{-3} min^{-1}, respectively). The catalytic efficiency is comparable and even higher than those of non-noble metal catalysts reported in the literature (Table S1). Fig. 4c reveals that the catalytic efficiency of Ni/Ni(OH)$_2$ could be further improved by increasing the reaction temperature to 40 and 60 °C. Based on the initial reaction rate, the calculated apparent activation energy (Ea) of Ni/Ni(OH)$_2$ is about 42.3 kJ·mol^{-1} (Fig. 4d), which is much lower than that of Ni(OH)$_2$ and Ni-NPs (the value is 78.8 kJ·mol^{-1} and 57.1 kJ·mol^{-1}, respectively).

Apart from the excellent activity, the stability and recyclability of Ni/Ni(OH)$_2$ are of vital importance for its practical application. No subsequent conversion of 4-NP was detected after removing the solid catalyst in the filtration test, confirming the heterogeneous nature of this catalyst (Fig. 5a). Moreover, by taking advantage of the superparamagnetic properties of Ni/Ni(OH)$_2$, a series of repeat catalytic experiments were carried out. As shown in Fig. 5b, Ni/Ni(OH)$_2$ displayed high reusability in the hydrogenation of 4-NP, in which it could recycled at least ten cycles without obvious
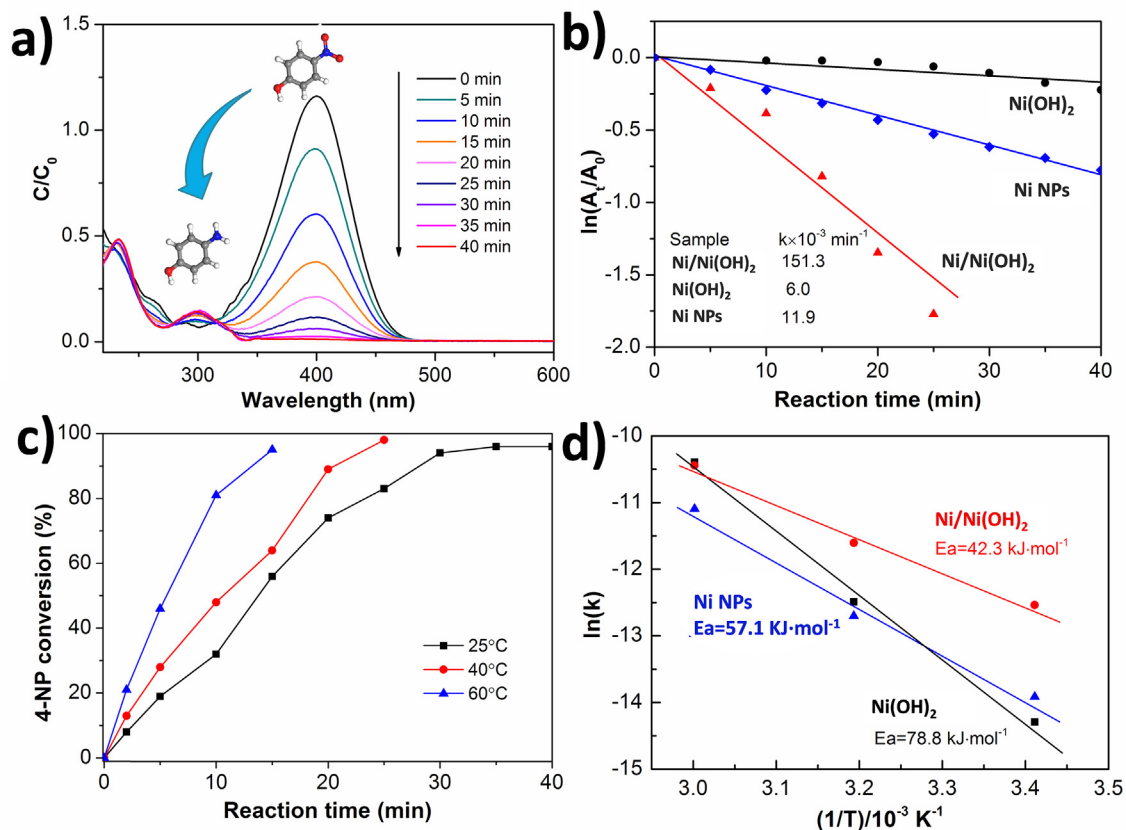
Fig. 4. Catalytic performance of the obtained catalysts: (a) UV–Vis spectra during hydrogenation of 4-NP in the presence of Ni/Ni(OH)$_2$. (b) Plot of ln (A$_t$/A$_0$) versus reaction time for the hydrogenation of 4-NP over the synthesized Ni-based catalysts. (c) Effects of the reaction temperature on the catalytic performance of Ni/Ni(OH)$_2$ in hydrogenation of 4-NP. (d) Apparent activation energy (Ea) of the reaction over Ni/Ni(OH)$_2$, Ni(OH)$_2$ and Ni NPs catalysts.
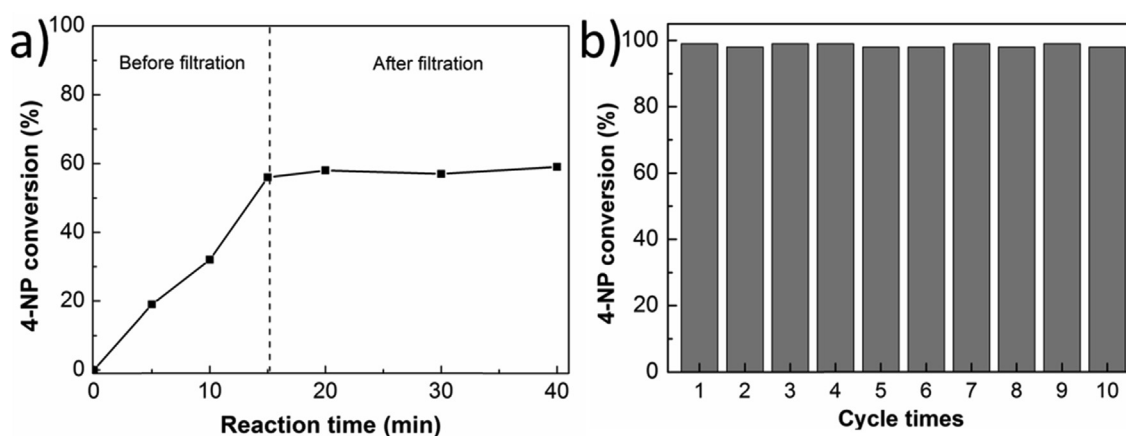
Fig. 5. (a) Leaching experiment by continuing the reaction after filtration of the Ni/Ni(OH)$_2$ catalysts and (b) the reusability performance of Ni/Ni(OH)$_2$ in the reduction of 4-NP for ten successive cycles.

fading in catalytic efficiency. The good reusability should be correlated to the relatively high stability of Ni/Ni(OH)$_2$. As displayed in Fig. S4, no obvious increase and/or change of the diffraction peak corresponding to metallic Ni phase was found in the XRD pattern of Ni/Ni(OH)$_2$ catalyst even after ten cycles. Meanwhile, the SEM image of the reused catalyst (Fig. S5) revealed no obvious collapse and transformation of the hierarchical structure, demonstrating a high reusability of Ni/Ni(OH)$_2$ during reaction.

4. Conclusions

In summary, a kind of Ni NPs embedded in a mesoporous Ni (OH)$_2$ architecture has been prepared by a solid-state redox strategy. It provides dual advantages as a robust catalyst and a magnetically recoverable entity for the hydrogenation of 4-nitrophene under mild conditions. The synergistic effect of homodispersed Ni NPs, high surface area and interconnected structure should be

responsible for its excellent performance. It could expose more active sites and facilitate the transport of reactants, leading to a relative high efficiency and low activation energy under mild conditions. The unique composition and structure of obtained material are expected to have a wider range of utilities, such as supercapacitor, electrode, or optic memory. Moreover, the synthesis route is facile, cost-effective, and scalable, and it has the potential to be extended to fabricating with other transition metals (for example Fe, Co, Cu, *etc.*) in hierarchical architectures.

Acknowledgements

Appendix A. Supplementary data

Supplementary data to this article can be found online at https://doi.org/10.1016/j.poly.2019.02.045.

References

[1] R.V. Jagadeesh, K. Murugesan, A.S. Alshammari, H. Neumann, Science 358 (2017) 326.
[2] G. Chen, C. Xu, X. Huang, J. Ye, L. Gu, G. Li, Z. Tang, B. Wu, H. Yang, Z. Zhao, Z. Zhou, G. Fu, N. Zheng, Nat. Mater. 15 (2016) 564.
[3] L. Geng, J. Song, Y. Zhou, Y. Xie, J. Huang, W. Zhang, L. Peng, G. Liu, Chem. Commun. 52 (2016) 13495.
[4] M. Tian, X. Cui, M. Yuan, J. Yang, J. Ma, Z. Dong, Green Chem. 19 (2017) 1548.
[5] M. Shokouhimehr, K. Hong, T.H. Lee, C.W. Moon, S.P. Hong, K. Zhang, J.M. Suh, K.S. Choi, R.S. Varma, H.W. Jang, Green Chem. 20 (2018) 3809.
[6] L. Sun, Y. Yin, F. Wang, W. Su, L. Zhang, Dalton Trans. 47 (2018) 4315.
[7] K. Layek, M.L. Kantam, M. Shirai, D. Nishio-Hamane, T. Sasaki, H. Maheswaran, Green Chem. 14 (2012) 3164.
[8] E. Menumerov, R.A. Hughes, S. Neretina, Catal. Sci. Technol. 7 (2017) 1460.
[9] L. Jin, X. Zhao, J. Ye, X. Qian, M. Dong, Catal. Commun. 107 (2018) 43.
[10] D. Li, Y. Nakagawa, K. Tomishige, Chin. J. Catal. 33 (2012) 583.
[11] J. Liang, P. Li, X. Zhao, Z. Liu, Q. Fan, Z. Li, J. Li, D. Wang, Nanoscale 10 (2018) 1383.
[12] M. Chai, X. Liu, L. Li, G. Pei, Y. Ren, Y. Su, H. Cheng, A. Wang, T. Zhang, Chin. J. Catal. 38 (2010) 1338.
[13] N. Ji, T. Zhang, M. Zheng, A. Wang, H. Wang, X. Wang, J.G. Chen, Angew. Chem. Int. Ed. 47 (2008) 8510.
[14] E. Kordouli, B. Pawelec, C. Kordulis, A. Lycourghiotis, J.L.G. Fierro, Appl. Catal. B: Environ. 238 (2018) 147.
[15] C. Li, G. Xu, Y. Zhai, X. Liu, Y. Ma, Y. Zhang, Fuel 203 (2017) 23.
[16] T. Sichumsaeng, N. Chanlek, S. Maensiri, Appl. Surf. Sci. 446 (2018) 177.
[17] C.-J. Wang, T.-C. Chen, J.-H. Lin, P.-R. Huang, H.-J. Tsai, C.-S. Chen, J. Colloid Interface Sci. 440 (2015) 179.
[18] Y. Wu, X. Wu, Q. Liu, C. Huang, X. Qiu, Int. J. Hydrogen Energy 42 (2017) 16003.
[19] Y. Liu, K. Zhang, W. Li, J. Ma, G.J. Vancso, J. Mater. Chem. A 6 (2018) 7741.
[20] R. Morales, C.H. Campos, J.L.G. Fierro, M.A. Fraga, G. Pecchi, Catal. Today 310 (2018) 59.
[21] T. Chen, S. Guo, J. Yang, Y. Xu, J. Sun, D. Wei, Z. Chen, B. Zhao, W. Ding, ChemPhysChem 18 (2017) 3454.
[22] T. Fu, M. Wang, W. Cai, Y. Cui, F. Gao, L. Peng, W. Chen, W. Ding, ACS Catal. 4 (2014) 2536.
[23] X. Guo, H. Kan, X. Liu, H. Geng, L. Wang, RSC Adv. 8 (2018) 15999.
[24] H. Qiu, F. Qiu, X. Han, J. Li, J. Yang, Appl. Surf. Sci. 407 (2017) 509.
[25] E. Soghrati, C. Choong, C.K. Poh, S. Kawi, A. Borgna, ChemCatChem 9 (2017) 1402.
[26] S. Zhu, J. Li, L. Ma, L. Guo, Q. Li, C. He, E. Liu, F. He, C. Shi, N. Zhao, ACS Appl. Mater. Interfaces 8 (2016) 11720.
[27] S. Zhu, J. Li, X. Deng, C. He, E. Liu, F. He, C. Shi, N. Zhao, Adv. Funct. Mater. 27 (2017) 1605017.
[28] Y. Teng, X.-D. Wang, J.-F. Liao, W.-G. Li, H.-Y. Chen, Y.-J. Dong, D.-B. Kuang, Adv. Funct. Mater. 28 (2018) 1802463.
[29] K. Tomishige, D. Li, M. Tamura, Y. Nakagawa, Catal. Sci. Technol. 7 (2017) 3952.
[30] R. Pavul Raj, S. Mohan, S.K. Jha, Chem. Commun. 52 (2016) 1930.
[31] Y. Zhu, W. Chu, N. Wang, T. Lin, W. Yang, J. Wen, X.S. Zhao, RSC Adv. 5 (2015) 77958.
[32] L. Geng, B. Zheng, X. Wang, W. Zhang, S. Wu, M. Jia, W. Yan, G. Liu, ChemCatChem 8 (2016) 805.
[33] L. Geng, M. Zhang, W. Zhang, M. Jia, W. Yan, G. Liu, Catal. Sci. Technol. 5 (2015) 3097.
[34] B. Zheng, S. Wu, X. Yang, M. Jia, W. Zhang, G. Liu, ACS Appl. Mater. Interfaces 8 (2016) 26683.
[35] L. Tao, C.-Y. Lin, S. Dou, S. Feng, D. Chen, D. Liu, J. Huo, Z. Xia, S. Wang, Nano Energy 41 (2017) 417.
[36] C. Zhang, L. Qian, K. Zhang, S. Yuan, J. Xiao, S. Wang, J. Mater. Chem. A 3 (2015) 10519.
[37] Q. Zhang, T. Jiang, B. Li, T. Wang, X. Zhang, Q. Zhang, L. Ma, ChemCatChem 4 (2012) 1084.
[38] L. Geng, X. Zhang, W. Zhang, M. Jia, G. Liu, Chem. Commun. 50 (2014) 2965.
[39] L. Geng, J. Song, B. Zheng, S. Wu, W. Zhang, M. Jia, G. Liu, Chin. J. Catal. 37 (2016) 1451.
[40] Y. Lu, L. Yu, M. Wu, Y. Wang, X.W. Lou, Adv. Mater. 30 (2018) 1702875.
[41] J. Huang, J. Chen, T. Yao, J. He, S. Jiang, Z. Sun, Q. Liu, W. Cheng, F. Hu, Y. Jiang, Z. Pan, S. Wei, Angew. Chem. Int. Ed. 54 (2015) 8722.
[42] X. Zhang, N. Wang, L. Geng, J. Fu, H. Hu, D. Zhang, B. Zhu, J. Carozza, H. Han, J. Colloid Interface Sci. 512 (2018) 844.
[43] L. Dou, Y. Wang, Y. Li, H. Zhang, Dalton Trans. 46 (2017) 15836.
[44] Y. Li, Y. Cao, D. Jia, J. Mater. Chem. A 2 (2014) 3761.
[45] X. Zhang, J. Fu, D.-S. Zhang, L. Geng, Polyhedron 146 (2018) 12.